J Biomol NMR (2009) 44:235–244
DOI 10.1007/s10858-009-9335-x

ARTICLE

Numerical design of RN_n^ν symmetry-based RF pulse schemes for recoupling and decoupling of nuclear spin interactions at high MAS frequencies

Christian Herbst · Jirada Herbst · Jörg Leppert · Oliver Ohlenschläger · Matthias Görlach · Ramadurai Ramachandran

Received: 31 March 2009 / Accepted: 3 June 2009 / Published online: 26 June 2009
© Springer Science+Business Media B.V. 2009

Abstract An approach for the efficient implementation of RN_n^ν symmetry-based pulse schemes that are often employed for recoupling and decoupling of nuclear spin interactions in biological solid state NMR investigations is demonstrated at high magic-angle spinning frequencies. RF pulse sequences belonging to the RN_n^ν symmetry involve the repeated application of the pulse sandwich $\{R_\phi R_{-\phi}\}$, corresponding to a propagator $U_{RF} = \exp(-i4\phi I_z)$, where $\phi = \pi\nu/N$ and R is typically a pulse that rotates the nuclear spins through 180° about the x-axis. In this study, broadband, phase-modulated 180° pulses of constant amplitude were employed as the initial 'R' element and the phase-modulation profile of this 'R' element was numerically optimised for generating RN_n^ν symmetry-based pulse schemes with satisfactory magnetisation transfer characteristics. At representative MAS frequencies, RF pulse sequences were implemented for achieving ^{13}C–^{13}C double-quantum dipolar recoupling and through bond scalar coupling mediated chemical shift correlation and evaluated via numerical simulations and experimental measurements. The results from these investigations are presented here.

Keywords MAS · Solid state NMR · Chemical shift correlation · Symmetry-based RF pulse schemes

Introduction

Magic-angle spinning (MAS) solid state NMR is emerging as an important tool for the structural characterisation of isotopically labelled biological systems. Although dipolar interactions between low γ nuclei are typically averaged out under MAS conditions, a variety of techniques have been reported for inhibiting the spatial averaging of weak dipolar couplings (Bennett et al. 1994; Griffin 1998; Dusold and Sebald 2000; Baldus 2002). This opened up the possibilities for achieving resonance assignments and the extraction of structural constraints such as internuclear distances and torsion angles. In addition to through-space dipolar-driven ^{13}C–^{13}C correlation experiments, through-bond scalar-coupling mediated MAS chemical shift correlation spectroscopy (TOBSY) (Baldus and Meier 1996; Heindrichs et al. 2001; Chan and Brunklaus 2001; Hardy et al. 2003; Leppert et al. 2004; Riedel et al. 2007) has also been found to be useful in solid state NMR structural studies of biological systems (Agarwal and Reif 2008; Detken et al. 2001). For the recoupling and decoupling of nuclear spin interactions in rotating solids and for achieving the evolution of the spins under the average Hamiltonian of interest, a symmetry-based approach has been developed by Levitt and co-workers (Carravetta et al. 2000; Levitt 2002). This makes use of the rotational properties of the nuclear spin interactions and involves the application of rotor-synchronised RF pulse sequences. Two classes of symmetry-based pulse sequences, denoted as CN_n^ν and RN_n^ν, have been introduced till date. The CN_n^ν class of RF

Electronic supplementary material The online version of this article (doi:10.1007/s10858-009-9335-x) contains supplementary material, which is available to authorized users.

C. Herbst · J. Leppert · O. Ohlenschläger · M. Görlach · R. Ramachandran (✉)
Research group Biomolecular NMR spectroscopy,
Leibniz Institute for Age Research, Fritz Lipmann Institute,
07745 Jena, Germany
e-mail: raman@fli-leibniz.de

J. Herbst
Department of Mathematics, Statistics and Computer,
Faculty of Science, Ubon Ratchathani University,
Ubon Ratchathani 34190, Thailand

pulse scheme involves the application of a basic element "C" corresponding to an RF cycle with unity propagator U_{RF} $(\tau_c) = \pm 1$. N such cycles are applied over n rotor periods τ_r. Successive C elements are incremented in phase by $\nu 2\pi/N$. RN_n^ν symmetry-based sequences, which are of interest in this study, involve the application of the pulse sandwich $\{R_\phi R_{-\phi}\}$, corresponding to a propagator $U_{RF} = \exp(-i4\phi I_z)$, where $\phi = \pi\nu/N$ and R is typically a pulse that rotates the nuclear spins through 180° about the x-axis. The pulse sandwich $\{R_\phi R_{-\phi}\}$ is repeated $N/2$ times over n rotor periods so as to form an RF cycle with unity propagator U_{RF} $(\tau_c) = \pm 1$. N, n and ν are all integers and appropriate values for these are chosen, via the selection rules for CN_n^ν and RN_n^ν symmetry, to generate the desired average Hamiltonian.

Symmetry-based RF pulse sequences have found a variety of applications in MAS NMR studies of biological systems and at any given MAS frequency it is possible to employ different RN_n^ν symmetries for generating the desired average Hamiltonian (Levitt 2002). For example, symmetries such as $R18_{16}^{-8}$, $R18_{16}^{1}$, $R18_{14}^{2}$, $R16_{14}^{1}$, $R30_{8}^{-4}$, $R14_{2}^{6}$ and $R20_{18}^{-9}$ are available for achieving CSA compensated γ-encoded homonuclear DQ dipolar recoupling (Carravetta et al. 2001; Kristiansen et al. 2002). The performance of RN_n^ν symmetry-based schemes critically depends on the choice of "R" and R elements such as $\{(\pi/2)_0(3\pi/2)_\pi\}$, $(\pi)_0$ and $\{(\pi/3)_0(5\pi/3)_\pi(\pi/3)_0\}$ are commonly employed in implementing RN_n^ν class of sequences. One of the difficulties with symmetry-based RF pulse schemes based on conventional rectangular RF pulses, however, is that the RF field strength requirement is related to the spinning speed. This can result in a situation where the RF field strength needed can become either too large that is beyond the hardware limits or too small that would lead to poor performance over a large bandwidth. Additionally, it is also possible that even when the RF field strength requirement can be satisfactorily met, the performance of the symmetry under consideration may not be satisfactory (Kristiansen et al. 2002). Such difficulties impeding the wider application of symmetry-based RF pulse schemes in biomolecular MAS solid state NMR investigations can be overcome, in principle, by employing phase and/or amplitude modulated basic elements that are tailor made taking into consideration the symmetry, the experimental requirements and constraints such as available RF power, MAS frequency and resonance offset range of the nuclei. Such an approach was successfully adopted in our recent work dealing with the generation of CN_n^ν symmetry-based pulse schemes (Herbst et al. 2009). In continuation of these studies, the numerical design of efficient RN_n^ν symmetry-based pulse schemes, e.g., for ^{13}C–^{13}C double-quantum dipolar recoupling and through-bond scalar coupling mediated chemical shift correlation, has been examined at high MAS frequencies in this work. The performance characteristics of the sequences generated were assessed via numerical simulations and experimental measurements. The results from these investigations are reported here.

Numerical and experimental procedures

RN_n^ν symmetry-based pulse schemes for ^{13}C–^{13}C DQ recoupling were implemented considering simultaneous application of ^1H decoupling during mixing. At long mixing times, as commonly required for scalar coupling mediated magnetisation transfers, it is well known that insufficient mismatch between the ^{13}C and ^1H RF field strengths can lead to substantial signal losses due to RF field interferences. Hence, to eliminate RF field interferences completely, optimised TOBSY pulse schemes were generated without simultaneous ^1H decoupling. Broadband, phase-modulated 180° pulses of constant amplitude with appropriate duration, as determined by the symmetry and MAS frequency, were first generated considering a simple spin 1/2 system. The global optimisation procedure "genetic algorithms" (GA) (Goldberg 1989; Forrest 1993; Judson 1997; Haupt and Haupt 2004; Freeman and Wu 1987; Wu and Freeman 1989; Xu et al. 1992; Herbst et al. 2009) was employed in generating the 180° pulses so as to obtain the propagator, $\exp(i\pi I_x)$, over a range of resonance offsets. The GA program package GAlib (Wall 1996), as employed in our recent study (Herbst et al. 2009), was used. Typically, a population size of 500 and 500 generations were used in the GA calculations. The pulses were implemented, unless mentioned otherwise, as a sandwich of a small number of pulses of equal duration, typically in the range of 0.5–2.0 μs. RF field strengths employed were either in the range of 40–50 kHz or 100–120 kHz depending on whether the pulses have to be used for implementing symmetry-based schemes with or without simultaneous ^1H decoupling. 180° pulses were constructed such that the phase modulation profile is symmetric with respect to the center of the pulse. These GA derived 180° pulses were used as the starting R element in implementing different RN_n^ν symmetry-based pulse schemes. The phase-modulation profile of the R element was further numerically optimised (see below) via the nonlinear least-squares optimisation procedure NL2SOL implemented in the SPINEVOLUTION program (Veshtort and Griffin 2006) so as to achieve, with the RF field strength available, the best possible performance of the symmetry-based scheme over the resonance offset range of the ^{13}C nuclei. The local optimisation run was repeated several times varying all the independent RF phase-values randomly over a range of ±10% and, if needed, without restricting the phase-modulation profile of the R element to be symmetric with

respect to the center of the pulse. These calculations were carried out employing a variety of computer systems, including a unix cluster with 64 processors, neglecting RF field inhomogeneities and considering initially only a limited number of 32 crystallite orientations selected according to the Zaremba-Cheng-Wolfsberg (ZCW) method (Cheng et al. 1973). Starting with the solution thus obtained a final stage of optimisation was generally carried out considering a slightly larger number, typically 84, of crystallite orientations. A Zeeman field strength corresponding to a ^{1}H resonance frequency of 500 MHz and representative spinning speeds were employed in this study. Typical chemical shift, scalar and dipolar coupling parameters of alanine aliphatic carbons were used in the numerical design.

As representative examples, symmetries such as $R18^{-8}_{16}$, $R18^{1}_{16}$, $R18^{-7}_{14}$, $R18^{2}_{14}$, $R16^{1}_{14}$, $R16^{-7}_{14}$, $R14^{-6}_{12}$, $R14^{1}_{12}$, $R20^{1}_{18}$ and $R20^{-9}_{18}$ (Kristiansen et al. 2002) were examined at a spinning speed of 25 kHz for achieving γ-encoded ^{13}C–^{13}C DQ recoupling. The $R32^{3}_{28}$ symmetry (Riedel et al. 2007) was employed for generating scalar coupling mediated ^{13}C–^{13}C chemical shift correlation (TOBSY) at spinning speeds of 33.333 and 25 kHz. Symmetry-based schemes with and without simultaneous application of ^{1}H decoupling were generated, respectively, with a two spin ^{13}C1–^{13}C2 and a four spin ^{1}H1–^{13}C1–^{13}C2–^{1}H2 system and with a resonance offset range of $\pm$10 kHz and $\pm$15 kHz. Since the initial rate of transfer of magnetisation from one spin to another is a measure of the efficacy of the mixing sequence, with a faster transfer representing an efficient dipolar or scalar coupling mediated magnetisation transfer, optimised RF pulse schemes were generated in this study by monitoring the magnitude of longitudinal magnetisation transferred to the second carbon spin as a function of the mixing time, starting with z magnetisation on the first carbon spin at zero mixing time. It is seen via numerical simulations that with DQ recoupling sequences such as the $R14^{6}_{2}$ (Carravetta et al. 2001), in a simple system of two directly coupled ^{13}C nuclei, the magnitude of the longitudinal magnetisation transferred to the second ^{13}C spin ($I_{1z} \rightarrow -I_{2z}$) typically reaches its maximum at $\sim$1 ms. Hence, broadband DQ recoupling sequences were developed by maximising the magnitude of the longitudinal magnetisation transferred to the second ^{13}C spin at $\sim$1 ms over the resonance offset range of the two nuclei. For TOBSY without simultaneous ^{1}H decoupling during mixing, the phase-modulation profile of the R element employed in the $R32^{3}_{28}$ symmetry scheme was optimised so as to achieve complete magnetisation transfer from one carbon to another, ($I_{1z} \rightarrow I_{2z}$), at $\tau_{mix} = (1/2J_{cc})$, over the resonance offset range of the two nuclei. The optimisation calculation was carried out in several stages with the ^{13}C–^{1}H dipolar coupling strength (set to 20 kHz, corresponding to a ^{13}C–^{1}H distance of $\sim$1.14 Å) raised gradually in several steps: 0, 2, 5, 10, 15 and 20 kHz, as in our earlier study. At every stage, to arrive at the best possible phase-modulation profile, the local optimisation run was repeated several times varying all the independent RF phase-values randomly over a range of $\pm$10%. The phase-modulation profile obtained at the end of every stage was used as the starting input for the subsequent stage of optimisation.

All simulations to assess the performance characteristics of the pulse sequences were carried out with the SPINEVOLUTION program (Veshtort and Griffin 2006) considering 168 α and β powder angles selected according to the REPULSION scheme (Bak and Nielsen 1997) and 16 γ angles. Chemical shift correlation experiments via longitudinal magnetisation exchange were carried out via standard procedures using a polycrystalline sample of (^{13}C,^{15}N) labelled samples of histidine on a 500 MHz wide-bore Bruker Avance III solid state NMR spectrometer equipped with a 2.5 mm triple resonance probe with the cooling air kept at a temperature of ~ -50°C. High power ^{1}H SPINAL64 (Fung et al. 2000; De Paepe et al. 2003) decoupling (γH_1 $\sim$120 kHz) was applied during mixing, if needed, and during acquisition.

Results and discussion

Figure 1 shows, as *representative* examples, the phase-modulation profiles and the performance characteristics of some of the GA derived 180° pulses generated considering different inversion bandwidths. Plots in Fig. 1a–h correspond to 180° pulses of 35 μs duration generated as a sandwich of 20 pulses of equal duration with an RF field strength of 50 kHz. Plots in Fig. 1i–p correspond to 180° pulses of 25 μs duration generated as a sandwich of 20 pulses of equal duration with an RF field strength of 120 kHz. Typically, it was possible to generate these pulses in a very short time (<15 min). The phase modulated pulses are scalable, as in the case of conventional pulses, and the performance characteristics of the pulses were found to be not affected significantly by minor variations in the RF field strength. The simulated plots clearly demonstrate the potential of the GA approach for generating phase-modulated, broadband 180° pulses simply as a sandwich of a small number of short pulses of equal duration with each slice characterised by an RF phase value. Considering that these pulses were only being used as the starting point of the numerical optimisation procedure, no attempts were made to generate RF pulses with better performance characteristics, e.g., by optimising the population size and the number of generations.

Starting with different GA derived broadband 180° pulses, a large number of numerical optimisation runs were

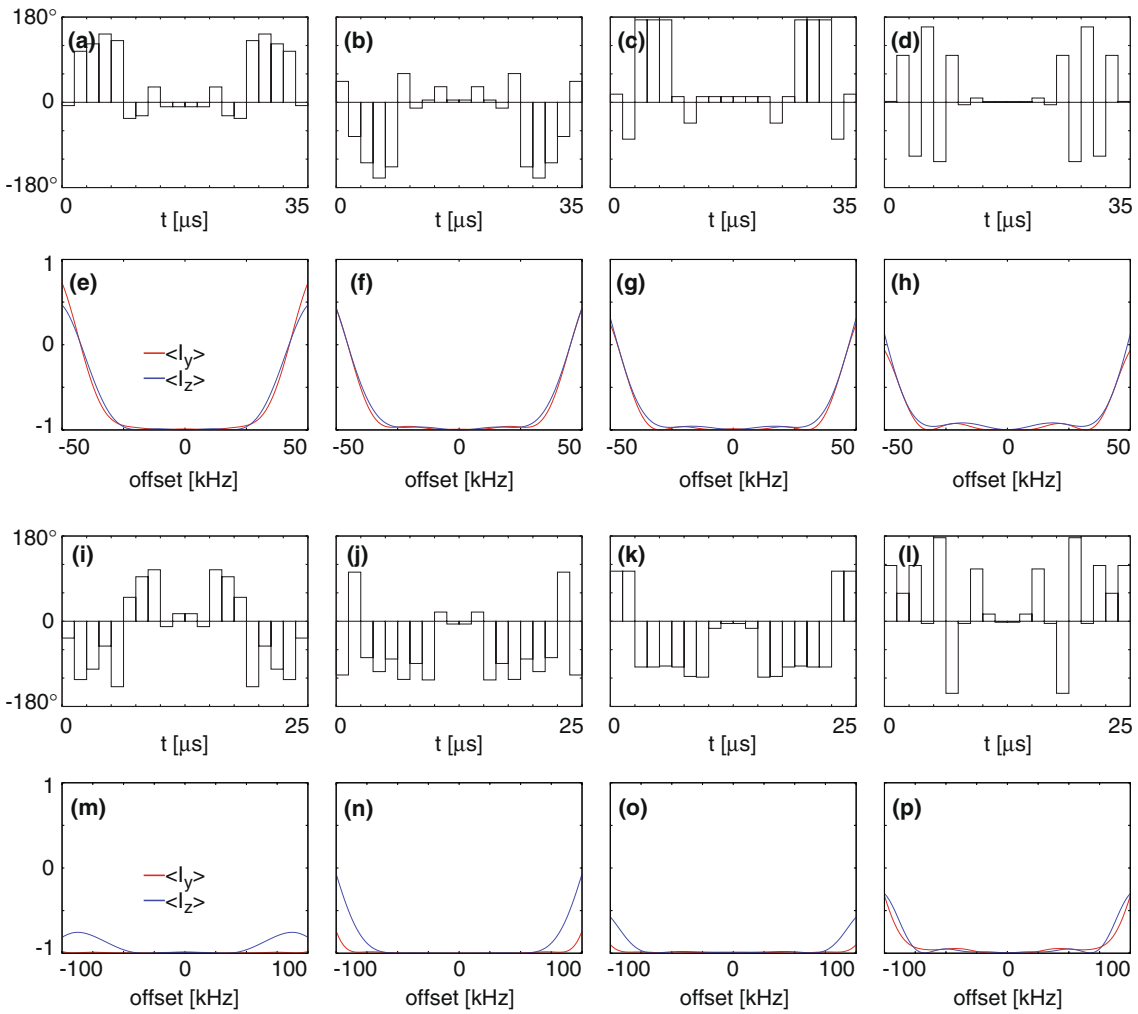

Fig. 1 GA derived broadband 180° pulses. RF phase values for the sandwich of 20 pulses of constant amplitude and equal duration constituting the 35 μs broadband 180° pulses generated considering an RF field strength of 50 kHz and inversion bandwidths of 40 kHz (**a**), 50 kHz (**b**), 60 kHz (**c**) and 70 kHz (**d**). The plots (**e**)–(**h**) show the corresponding performance characteristics of the different pulses, starting with I_z and I_y magnetisation components. RF phase values for the sandwich of 20 pulses of constant amplitude and equal duration constituting the 25 μs broadband 180° pulses generated considering an RF field strength of 120 kHz and inversion bandwidths of 80 kHz (**i**), 100 kHz (**j**), 120 kHz (**k**) and 140 kHz (**l**). The plots (**m**)–(**p**) show the corresponding inversion characteristics of the different pulses, starting with I_z and I_y magnetisation components. The RF phase values for the first 10 slices are given in the supplementary material

carried out for realising satisfactory performance of the symmetry under consideration. In general it was possible to generate, for each symmetry, a variety of optimised R elements leading to the satisfactory performance of the pulse sequence. Using a Mac Pro with four cores, typically, generation of RN_n^v symmetry-based schemes could be achieved in a short time (<1 h and <3 h for optimisation calculations carried out with and without ^{1}H decoupling, respectively). The simulated performance characteristics of some of the numerically designed RN_n^v symmetry-based DQ recoupling schemes are shown in Fig. 2 along with the phase-modulation profiles (a1)–(a4) of the basic R elements. The plots (b1)–(b4) show as a function of the mixing time the magnitude of longitudinal magnetisation transferred to the second carbon spin, starting with z magnetisation on the first carbon spin at zero mixing time. These plots were obtained using the chemical shift tensor and dipolar coupling parameters of alanine and glycine, with the ^{13}C carrier kept either at the center of the two resonances or at 110 ppm, as indicated. Although the optimised basic elements were generated employing CSA, scalar and dipolar coupling parameters corresponding to that of the $^{13}C^{\alpha}$ and $^{13}C^{\beta}$ nuclei of alanine, it is seen that reasonably satisfactory performance can also be obtained even in the situation where one of the carbons has a large CSA, as in the case of the $^{13}C^{\alpha} \rightarrow {}^{13}C'$ magnetisation transfer in peptides and proteins. This would permit satisfactory DQ recoupling in the entire ^{13}C spectral range at

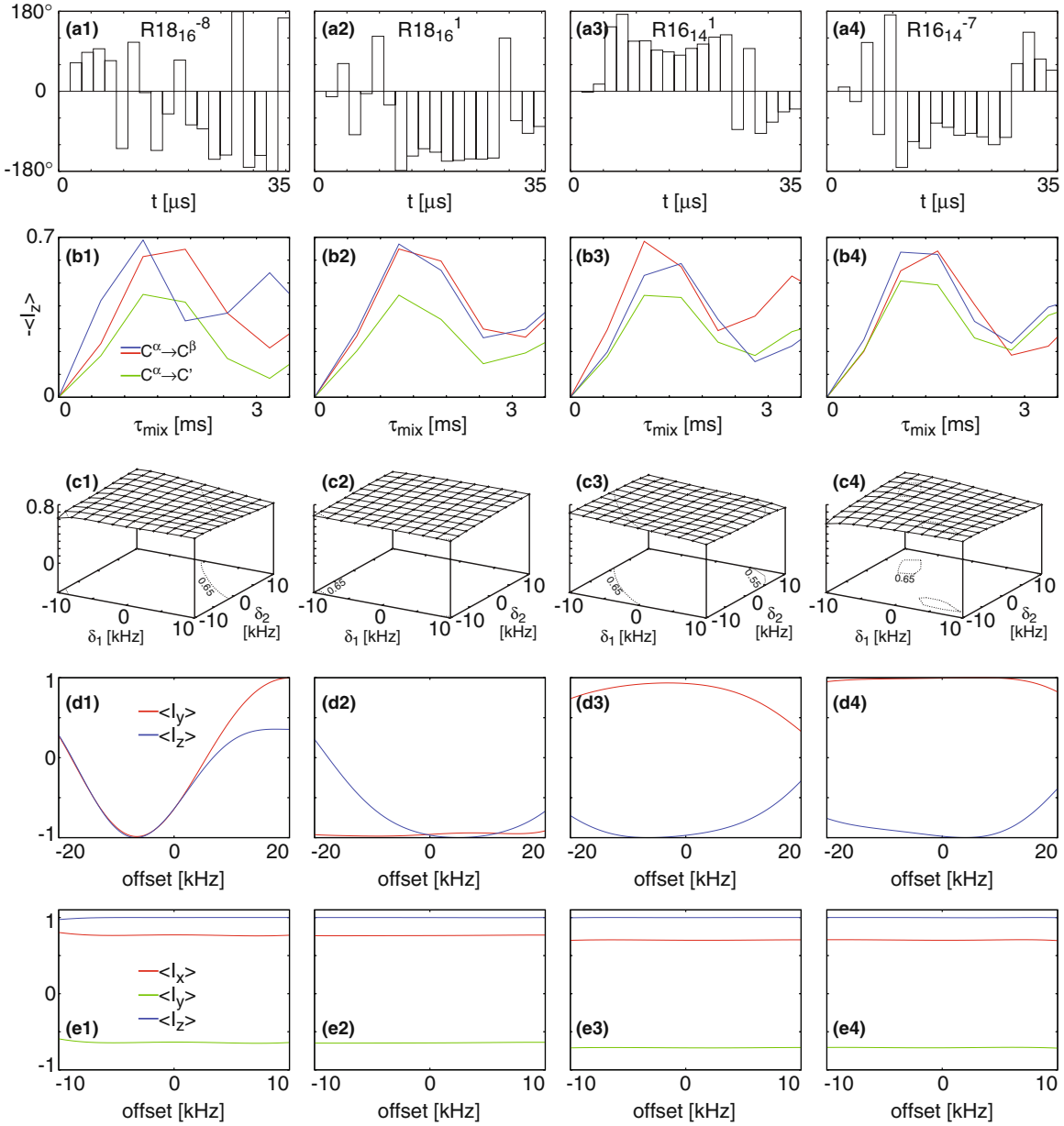

Fig. 2 Optimised R elements and the corresponding performance characteristics of the DQ recoupling schemes $R18_{16}^{-8}$ (**a1**)–(**e1**), $R18_{16}^{1}$ (**a2**)–(**e2**), $R16_{14}^{1}$ (**a3**)–(**e3**) and $R16_{14}^{-7}$ (**a4**)–(**e4**) generated at a MAS frequency of 25 kHz, employing, respectively, ^{13}C RF field strengths of 44, 49, 50 and 50 kHz. Plots (**a1**)–(**a4**) show, respectively, the phase-modulation profiles of the numerically optimised R elements obtained for the above mentioned symmetries. Plots (**b1**)–(**b4**) show the corresponding simulated longitudinal magnetisation transfer characteristics. These simulations, carried out at a Zeeman field strength corresponding to a ^{1}H resonance frequency of 500 MHz, show the magnitude of the transferred magnetisation (normalised to the maximum transferable signal) on the second carbon starting with z magnetisation on carbon 1. The simulations for the $C^{\alpha} \rightarrow C^{\beta}$ and $C^{\alpha} \rightarrow C'$ transfers were carried out using typical chemical shift, scalar and dipolar coupling parameters of alanine and glycine with the ^{13}C carrier kept either at the center of the two resonances (plot shown in *blue*) or at 110 ppm (*green* and *red*). Plots (**c1**)–(**c4**) show, as a function of the resonance offsets of the dipolar coupled nuclei, the magnitude of the transferred magnetisation on C^{β} at a τ_{mix} of $\sim$1.2 ms, starting with z magnetisation on C^{α} at zero mixing time. The plots (**d1**)–(**d4**) show the response following the application of the different R elements, starting with I_z and I_y magnetisation components. Starting with the I_z magnetisation component, the observed I_z magnetisation component following the application of the $\{R_{\phi}R_{-\phi}\}$ pulse sandwich are given in (**e1**)–(**e4**) (*blue line*). Starting with the I_x magnetisation component, the observed I_x and I_y magnetisation components following the application of the $\{R_{\phi}R_{-\phi}\}$ pulse sandwich are also given in (**e1**)–(**e4**) (*red* and *green line*, respectively). The phase shifted R elements R_{ϕ} and $R_{-\phi}$ were generated by adding and substracting, respectively, the phase value ϕ with respect to the starting R element. These plots (**d1**)–(**d4**) and (**e1**)–(**e4**) were generated as a function of the resonance offset considering a single spin-1/2 system. The RF phase values for the 20 slices of the R elements are given in the supplementary material

moderate Zeeman field strengths. The plots (c1)–(c4) show, as a function of the resonance offsets of the dipolar coupled nuclei, the magnitude of the transferred magnetisation on spin 2 at a τ_{mix} of $\sim$1.2 ms, starting with z magnetisation on the first carbon spin at zero mixing time. The performance characteristics of the sequences are found to be not very much dependent on the resonance offsets of the dipolar coupled nuclei. These data reveal that it is possible to implement efficient DQ recoupling schemes even at high MAS frequencies using only a moderate ^{13}C RF field strength of 50 kHz or less. It is worth noting that efficient RN_n^v symmetry-based DQ recoupling schemes could not be generated with R elements where the phase-modulation profile was restricted to be symmetric with respect to the center of the pulse. Hence, this restriction was lifted during the local optimisation calculations. Overall, the performance of the different RN_n^v symmetry-based DQ recoupling schemes investigated in this study using optimised R elements, at the spinning speed of 25 kHz, is found to be better than that can be realised with R elements of the type $\{(\pi/3)_0(5\pi/3)_\pi(\pi/3)_0\}$, $(\pi)_0$ and $\{(\pi/2)_0(3\pi/2)_\pi\}$ considered recently (Kristiansen et al. 2002) (data not shown). It is worth mentioning that the simulated performance characteristics of the numerically optimised R elements, Fig. (d1)–(d4), clearly suggest that these R elements do not necessarily belong to the class of pulses that rotate the nuclear spins through 180° about the x-axis. However, the $\{R_\phi R_{-\phi}\}$ pulse sandwiches formed with these optimised R elements correspond, as seen from the performance characteristics (e1)–(e4), to the propagator $U_{RF} = \exp(-i4\phi I_z)$ over the resonance offset range considered. This implies that it is not necessary to restrict, as we have done, the starting input to the local optimisation calculations to RF pulses that rotate the nuclear spins through 180° about the x-axis.

The TOBSY magnetisation transfer characteristics observed with the $R32_{28}^3$ symmetry-based scheme at spinning speeds of 33.333 kHz (a1–d1, a2–d2, a5–d5) and 25 kHz (a3–d3, a4–d4) and without ^{1}H decoupling during mixing are shown in Fig. 3, along with the corresponding optimised R elements (a1)–(a5). The 1D magnetisation transfer plots (b1)–(b5) were obtained keeping the ^{13}C RF carrier at 110 ppm. In the case of $^{13}C^\alpha \rightarrow {}^{13}C^\beta$ transfer, the calculations were carried out considering a four-spin ^{1}H1–^{13}C1–^{13}C2–^{1}H2 system and employing CSA, scalar and dipolar coupling parameters corresponding to that of the $^{13}C^\alpha$ and $^{13}C^\beta$ nuclei of alanine. Similarly, in the case of $^{13}C^\alpha \rightarrow {}^{13}C'$ transfer, the calculations were carried out employing a three-spin ^{1}H1–^{13}C1–^{13}C2 system and using CSA, scalar and dipolar coupling parameters corresponding to that of $^{13}C^\alpha$ and $^{13}C'$ nuclei of glycine. 3D plots (c1)–(c5) and (d1)–(d5) show the magnetisation transfer characteristics as a function of the resonance offsets of the two nuclei involved. Other details are given in the figure caption. It is worth noting that although the optimised basic elements were generated employing CSA, scalar and dipolar coupling parameters corresponding to that of the $^{13}C^\alpha$ and $^{13}C^\beta$ nuclei of alanine, it is seen that satisfactory performance can be obtained even in the case of the $^{13}C^\alpha \rightarrow {}^{13}C'$ magnetisation transfer. In situations where an R element with a relatively short duration is required, it is seen from the present study that it is possible to generate efficient RN_n^v symmetry-based schemes employing R elements constructed simply as a sandwich of a small number of pulses of equal duration with each slice defined by a RF phase value. However, if the present approach will be time consuming or does not lead to a satisfactory solution, it is also possible to generate efficient RN_n^v symmetry-based schemes using R elements where the phase-modulation profile is defined in terms of a simple Fourier series (Herbst et al. 2009). As an example, (b5)–(d5) show the performance characteristics of the $R32_{28}^3$ symmetry-based scheme at the spinning speed of 33.333 kHz employing the optimised R element (a5) generated via the Fourier approach. As in the case of DQ recoupling, it is observed via numerical simulations that the optimised TOBSY R elements do not necessarily belong to the class of pulses which rotate the nuclear spins through 180° about the x-axis (data not shown). It is also observed (data not shown) that the overall performance of the $R32_{28}^3$ symmetry-based scheme with numerically optimised R element is also better than that can be realised using tanh/tan adiabatic pulses as the R element (Riedel et al. 2007).

The performance characteristics of the symmetry-based sequences reported here were assessed via experimental measurements and some representative data are given below. The 2D ^{13}C–^{13}C chemical shift correlation spectrum of a polycrystalline sample of histidine acquired with the $R18_{16}^{-8}$ symmetry is given in Fig. 4 along with some representative spectral cross-sections taken from this and other spectra acquired with RN_n^v symmetries employing optimised R elements reported here. As expected under DQ mixing, the spectra and spectral cross-sections clearly show the characteristic alternation of direct and relayed cross-peak intensities. As reflected by the corresponding cross-peak intensities, relayed magnetisation transfers are also seen even at the short τ_{mix} employed. Considering ^{13}C DQ recoupling RF field strength in the range of 40–50 kHz, we also acquired 2D ^{13}C–^{13}C chemical shift correlation spectra with different RN_n^v symmetries reported in the literature employing $\{(\pi/2)_0(3\pi/2)_\pi\}$ and $(\pi)_0$ as the R element. The corresponding spectral cross-sections taken from these spectra are also given. Overall, the DQ recoupling performance observed with RN_n^v symmetries employing numerically optimised R elements is seen to be superior. The TOBSY spectrum shown in Fig. 5a was obtained without

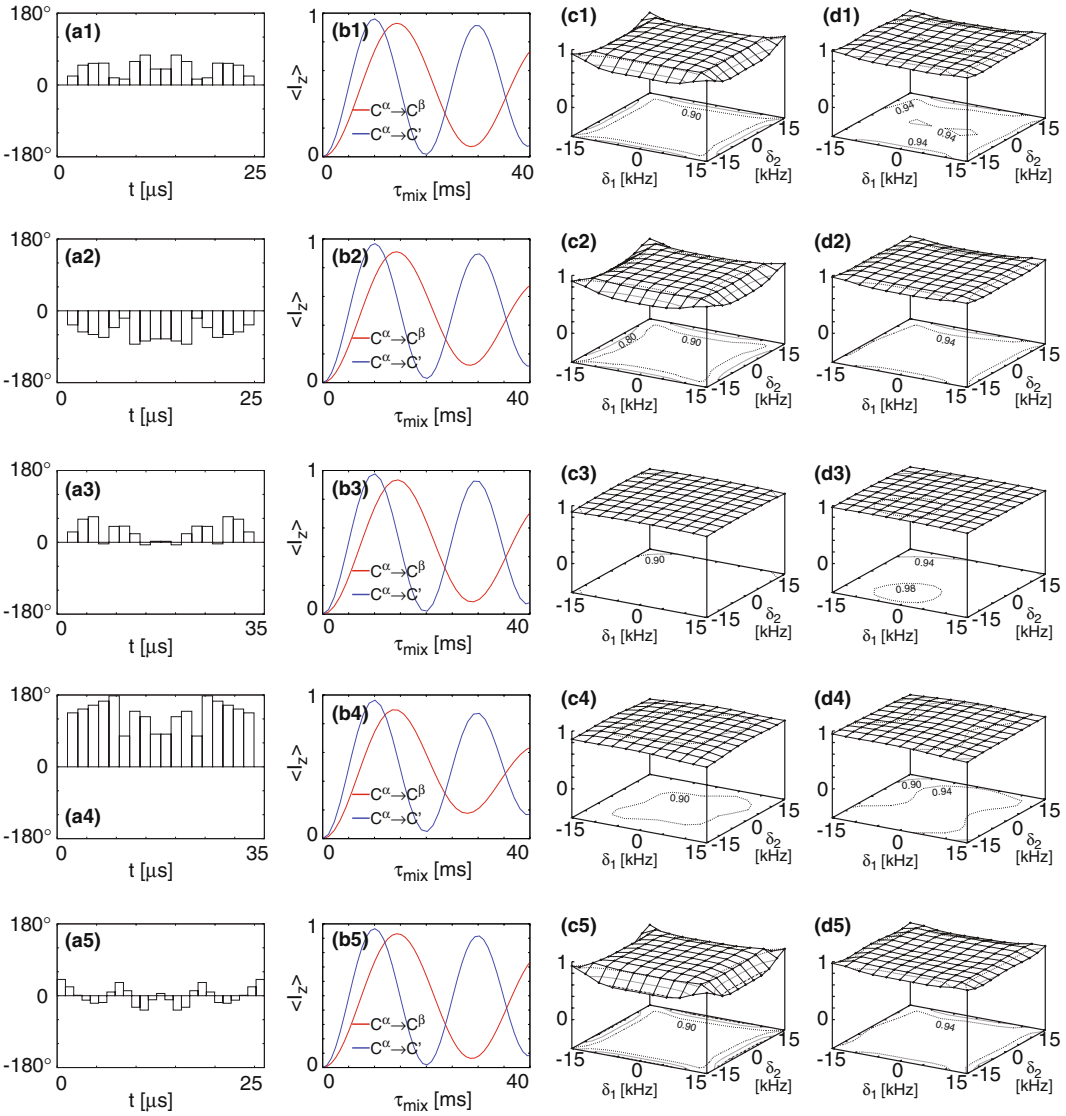

Fig. 3 The phase modulation profiles of optimised R elements with durations of 26.25 μs (**a1**, **a2**, **a5**) and 35 μs (**a3**, **a4**) and the corresponding simulated longitudinal magnetisation transfer characteristics, at a Zeeman field strength corresponding to a ^{1}H frequency of 500 MHz, observed with the $R32_{28}^{3}$ symmetry-based RF pulse scheme at spinning speeds of 33.333 kHz (**a1**–**d1**, **a2**–**d2**, **a5**–**d5**) and 25 kHz (**a3**–**d3**, **a4**–**d4**) without ^{1}H decoupling during mixing. The simulated plots in (**b1**)–(**b5**) show the magnitude of the transferred magnetisation (normalised to the maximum transferable signal) on the second carbon ($^{13}C^{\beta}/^{13}C'$) starting with z magnetisation on carbon 1 ($^{13}C^{\alpha}$). These plots were obtained keeping the ^{13}C RF carrier at 110 ppm using RF field strengths of 114 kHz (**b1**, **b2**, **b5**), 120 kHz (**b3**) and 100 kHz (**b4**). The $^{13}C^{\alpha} \rightarrow {}^{13}C^{\beta}$ simulations were carried out with a four-spin ^{1}H1–^{13}C1–^{13}C2–^{1}H2 system (with all the atoms in the same plane) employing CSA, scalar and dipolar coupling parameters corresponding to that of the $^{13}C^{\alpha}$ and $^{13}C^{\beta}$ nuclei of alanine. The $^{13}C^{\alpha} \rightarrow {}^{13}C'$ simulations were carried out with a three-spin ^{1}H1–^{13}C1–^{13}C2 system using CSA, scalar and dipolar coupling parameters corresponding to that of $^{13}C^{\alpha}$ and $^{13}C'$ nuclei of glycine. 3D plots **c1**–**c5** and **d1**–**d5** show the magnitude of the $^{13}C^{\alpha} \rightarrow {}^{13}C^{\beta}$ and $^{13}C^{\alpha} \rightarrow {}^{13}C'$ transfers, as a function of the resonance offsets of the two nuclei involved at mixing times of 14 ms (**c1**)–(**c5**) and 9.4 ms (**d1**)–(**d5**). A ^{13}C–^{1}H dipolar coupling strength of 20 kHz was employed in these simulations and the C–H bonds were assumed to be at angle of 109° with respect to the ^{13}C–^{13}C bond. The RF phase values for the first 10 slices of the R elements (**a1**)–(**a4**) are given in the supplementary material. The R element (**a5**) was generated via the Fourier approach with the phase modulation profile expressed as a cosine Fourier series: $\phi(t) = \Sigma a_n \cos(n\omega t)$, where $\omega = 2\pi/t_p$ is the modulation frequency with t_p corresponding to the pulse duration. This pulse was divided into 25 pulses of equal duration. The Fourier coefficients and the corresponding phase values for the first 13 slices are given in the supplementary material

^{1}H decoupling during mixing, with the $R32_{28}^{3}$ symmetry at a spinning speed of 33.333 kHz using the optimised R element given in Fig. 3a1. Representative spectral cross-sections taken from this and other spectra acquired employing different optimised R elements given in Fig. 3 are also presented to indicate spectral quality. Direct and

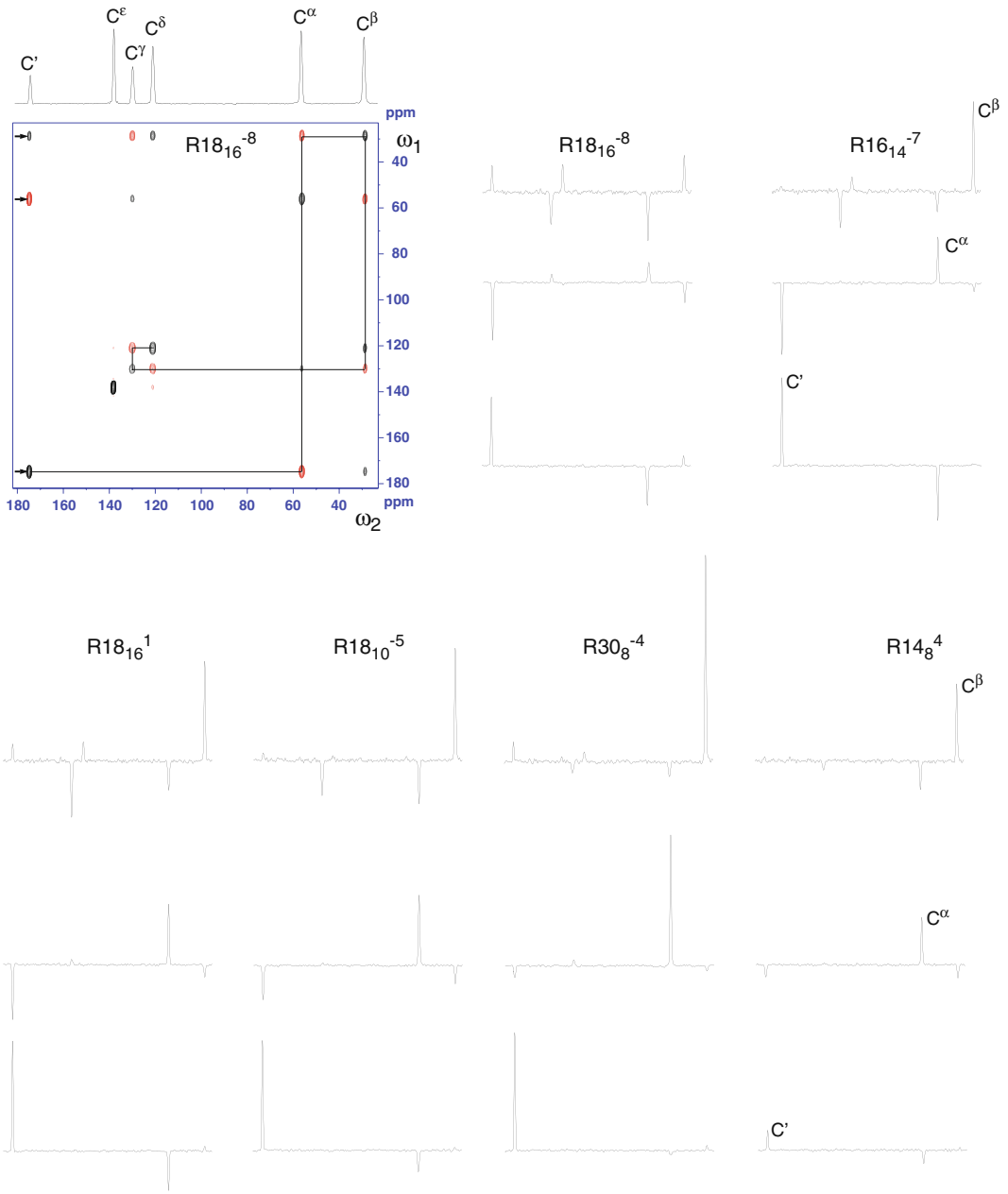

Fig. 4 2D ^{13}C–^{13}C chemical shift correlation spectrum of L-histidine hydrochloride obtained via longitudinal magnetisation transfer at a spinning speed of 25 kHz using $R18_{16}^{-8}$ DQ dipolar recoupling scheme. This spectrum was obtained employing a mixing time of 1.28 ms, the corresponding numerically optimised *R* element given in Fig. 2a1 and with ^{13}C RF field strength of 44 kHz. The spectrum was generated with 32 transients per t_1 increment, 64 t_1 increments, spectral width in the indirect dimension of 25,000 Hz and recycle time of 2 s, keeping the RF carrier at 100 ppm. A few representative cross-sections are also given to indicate spectral quality. The corresponding spectral cross-sections taken from data collected under similar experimental conditions using other symmetries are also given for comparison. The data with $R16_{14}^{-7}$ and $R18_{16}^{1}$ symmetries were collected employing the corresponding optimised *R* elements given in Fig. 2 with mixing times of 1.12 ms and 1.28 ms and RF field strengths of 50 and 49 kHz, respectively. The spectra with $R18_{10}^{-5}$, $R30_{8}^{-4}$ and $R14_{8}^{4}$ symmetries were collected employing the *R* elements $(\pi/2)_0(3\pi/2)_\pi$, $(\pi)_0$ and $(\pi/2)_0(3\pi/2)_\pi$ with mixing times of 1.2, 1.28 and 1.28 ms and RF field strengths of 45, 47 and 44 kHz, respectively. The C^{β} cross-sections are plotted with twice the vertical scale intensity compared to the C^{α} and C' cross-sections

relayed cross-peaks of appreciable intensities could be clearly seen in the spectra. Consistent with the results from numerical simulations, it is seen that RN_n^v symmetry-based TOBSY and DQ recoupling schemes can be effectively implemented for the study of isotopically labelled biological systems at fast MAS frequencies.

In conclusion, the present study demonstrates an approach for exploiting the full potential of the symmetry-

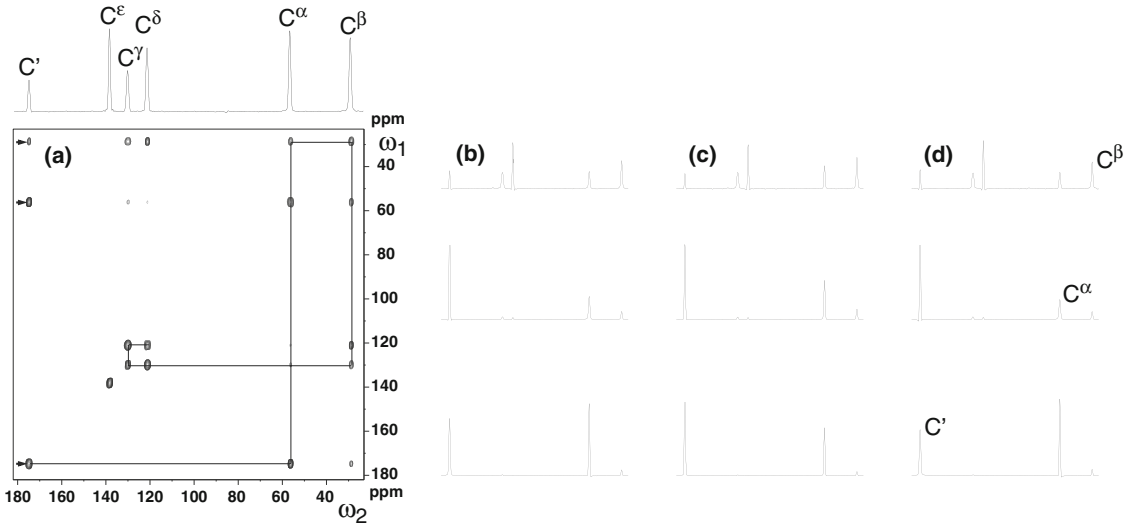

Fig. 5 2D ^{13}C–^{13}C scalar coupling mediated chemical shift correlation spectrum of L-histidine hydrochloride. The spectrum (**a**) was generated with the $R32_{28}^{3}$ symmetry, using the *R* element with the optimised phase-modulation profile given in Fig. 3a1, without ^{1}H decoupling during mixing, at a spinning speed of 33.333 kHz, with ^{13}C RF field strength of 114 kHz during mixing, a mixing time of 5.88 ms, 16 transients per t_1 increment, 128 t_1 increments, spectral width in the indirect dimension of 33.333 kHz, recycle time of 2 s and with the RF carrier kept at 100 ppm. A few representative cross-sections taken from this spectrum and spectra generated with other *R* elements are also given to indicate spectral quality. The cross-sections shown in (**b**, **c** and **d**) are taken from spectra generated employing *R* elements given in Fig. 3a1, a2, a5, respectively. The C^{β} cross-sections are plotted with twice the vertical scale intensity compared to the C^{α} and C′ cross-sections

based procedure for implementing efficient RN_n^{ν} symmetry-based pulse schemes that are commonly required in biomolecular MAS solid state NMR studies. It has been shown that by optimising the phase-modulation profile of the *R* element, that can be implemented, e.g., as a sandwich of a small number of pulses of equal duration with only a limited number of independent phase variables, it is possible to generate efficient pulse sequences taking into account experimental requirements and constraints. The approach outlined here will be useful in situations where it is difficult to implement efficient RN_n^{ν} symmetry-based pulse sequences employing conventional rectangular pulse based *R* elements. Extension of the present approach for designing pulse schemes for efficient magnetisation transfer in heteronuclear spin systems, e.g., ^{13}C–^{15}N, with or without simultaneous ^{1}H decoupling during mixing is conceivable and such studies are under way.

Acknowledgments This study has been funded in part by a grant from the Deutsche Forschungsgemeinschaft (GO474/6-1). The FLI is a member of the Science Association 'Gottfried Wilhelm Leibniz' (WGL) and is financially supported by the Federal Government of Germany and the State of Thuringia.

References

Agarwal V, Reif B (2008) Residual methyl protonation in perdeuterated proteins for multi-dimensional correlation experiments in MAS solid-state NMR spectroscopy. J Magn Reson 194:16–24

Bak M, Nielsen NC (1997) REPULSION, a novel approach to efficient powder averaging in solid state NMR. J Magn Reson 125:132–139

Baldus M (2002) Correlation experiments for assignment and structure elucidation of immobilized polypeptides under magic angle spinning. Prog Nucl Magn Reson Spectrosc 41:1–47

Baldus M, Meier BH (1996) Total correlation spectroscopy in the solid state. The use of scalar couplings to determine the through-bond connectivity. J Magn Reson A 121:65–69

Bennett AE, Griffin RG, Vega S (1994) NMR basic principles and progress, vol 33. Springer, Berlin, pp 1–77

Carravetta M, Eden M, Zhao X, Brinkmann A, Levitt MH (2000) Symmetry principles for the design of radiofrequency pulse sequences in the nuclear magnetic resonance of rotating solids. Chem Phys Lett 321:205–215

Carravetta M, Eden M, Johannessen OG, Luthman H, Verdegem PJE, Lugtenburg J, Sebald A, Levitt MH (2001) Estimation of carbon–carbon bond lengths and medium-range internuclear distances by solid-state nuclear magnetic resonance. J Am Chem Soc 123:10628–10638

Chan JCC, Brunklaus G (2001) R sequences for the scalar-coupling mediated homonuclear correlation spectroscopy under fast magic-angle spinning. Chem Phys Lett 349:104–112

Cheng VB, Suzukawa HH, Wolfsberg M (1973) Investigations of a nonrandom numerical method for multidimensional integration. J Chem Phys 59:3992–3999

De Paepe G, Lesage A, Emsley L (2003) The performance of phase modulated heteronuclear dipolar decoupling schemes in fast magic-angle-spinning nuclear magnetic resonance experiments. J Chem Phys 119:4833–4841

Detken A, Hardy EH, Ernst M, Kainosho M, Kawakami T, Aimoto S, Meier BH (2001) Methods for sequential resonance assignment in solid, uniformly ^{13}C, ^{15}N labelled peptides: quantification and application to antamanide. J Biomol NMR 20:203–221

Dusold S, Sebald A (2000) Dipolar recoupling under magic-angle spinning conditions. Annu Rep NMR Spectrosc 41:185–264

Forrest S (1993) Genetic algorithms—principles of natural-selection applied to computation. Science 261:872–878

Freeman R, Wu XL (1987) Design of magnetic resonance experiments by genetic evolution. J Magn Reson 75:184–189

Fung BM, Khitrin AK, Ermolaev K (2000) An improved broadband decoupling sequence for liquid crystals and solids. J Magn Reson 142:97–101

Goldberg DE (1989) Genetic algorithms in search, optimization and machine learning. Addison-Wesley publishing company, Massachusetts

Griffin RG (1998) Dipolar recoupling in MAS spectra of biological solids. Nat Struct Biol 5:508–512

Hardy EH, Detken A, Meier BH (2003) Fast-MAS total through-bond correlation spectroscopy using adiabatic pulses. J Magn Reson 165:208–218

Haupt RL, Haupt SE (2004) Practical genetic algorithms. Wiley-Interscience, Hoboken

Heindrichs ASD, Geen H, Giordani C, Titman JJ (2001) Improved scalar shift correlation NMR spectroscopy in solids. Chem Phys Lett 335:89–96

Herbst C, Herbst J, Kirschstein A, Leppert J, Ohlenschläger O, Görlach M, Ramachandran R (2009) Design of high-power, broadband 180° pulses and mixing sequences for fast MAS solid state chemical shift correlation NMR spectroscopy. J Biomol NMR 43:51–61

Judson R (1997) Genetic algorithms and their use in chemistry. In: Lipkowitz KB, Boyd DB (eds) Reviews in computational chemistry, vol 10. VCH Publishers, New York, pp 1–73

Kristiansen PK, Mitchell D, Evans JNS (2002) Double-quantum dipolar recoupling at high magic-angle spinning rates. J Magn Reson 157:253–266

Leppert J, Ohlenschläger O, Görlach M, Ramachandran R (2004) Adiabatic TOBSY in rotating solids. J Biomol NMR 29:167–173

Levitt MH (2002) Symmetry-based pulse sequences in magic-angle spinning solid-state NMR. In: Grant DM, Harris RK (eds) Encyclopedia of nuclear magnetic resonance. Wiley, Chichester

Riedel K, Herbst C, Leppert J, Ohlenschläger O, Görlach M, Ramachandran R (2007) Broadband homonuclear chemical shift correlation at high MAS frequencies: a study of tanh/tan adiabatic RF pulse schemes without ^{1}H decoupling during mixing. J Biomol NMR 37:277–286

Veshtort M, Griffin RG (2006) Spinevolution: a powerful tool for the simulation of solid and liquid state NMR experiments. J Magn Reson 178:248–282

Wall M (1996) GAlib: A C++ library of genetic algorithm components, version 2.4.7

Wu XL, Freeman R (1989) Darwin's ideas applied to magnetic resonance. The marriage broker. J Magn Reson 85:414–420

Xu P, Wu XL, Freeman R (1992) User-friendly selective pulses. J Magn Reson 99:308–322